

Jet substructure in pp collisions with ALICE

Ezra D. Lesser, on behalf of the ALICE Collaboration

UC Berkeley, Department of Physics, 366 Physics North, Berkeley, CA 94720-7300, USA

Jet substructure observables have been used by experiments at the Large Hadron Collider (LHC) as instruments to search for new physics as well as to study perturbative and non-perturbative processes in quantum chromodynamics (QCD). Some observables are infrared and collinear safe and thus easily comparable to first-principles calculations, while others offer direct insight into specific physical phenomena such as the quark-gluon plasma formed in heavy-ion collisions. The high-precision capability of the ALICE tracking system allows a unique opportunity at LHC energies to measure tracks with low transverse momentum, permitting high precision access to the softer components inside jets with an excellent angular resolution. We present some recent charged-particle jet substructure measurements in pp collisions with ALICE, including the generalized jet angularities, the angular jet axes differences, and the direct observation of the dead-cone effect in QCD using the primary Lund Plane. These results provide new insights into the evolution of jets by comparing ALICE measurements to predictions from different event generators and perturbative QCD calculations.

1 Introduction

In high-energy particle collisions, hadron jets are a direct consequence of quantum chromodynamics (QCD). These jets form from an initial hard (high Q^2) parton scattering, followed by a scale evolution culminating in hadronization near Λ_{QCD} . Jets can be experimentally defined from a set of measured tracks by using a jet reconstruction algorithm, such as a sequential recombination algorithm, along with a chosen resolution (radius) parameter. Jet substructure observables are then calculated from the jet's individual constituents, allowing characterization of the jet's internal radiation pattern. Some observables are constructed to enable direct calculations from first-principles QCD, permitting direct tests of theory. Jet substructure observables can additionally be tuned to explore nonperturbative processes such as hadronization.

Jet “grooming” procedures can be used to remove soft, wide-angle radiations and enhance perturbative calculability. One of the most popular grooming procedures is known as soft drop¹, which first reclusters jet constituents using the Cambridge-Aachen algorithm², producing a tree data structure that follows the expected angular ordering of emissions in QCD. One can then iterate through this tree, trimming away the outermost branches until the soft drop grooming condition, $\min(p_{T1}, p_{T2})/(p_{T1} + p_{T2}) > z_{\text{cut}} (\Delta R_{12}/R)^\beta$, is satisfied, where R is the jet radius, p_{T1} and p_{T2} are the transverse momenta of two branches at a particular vertex, ΔR_{12} is their distance in the rapidity-azimuth plane, and z_{cut} and β are user-defined parameters.

In these proceedings, each of the following three sections highlights a recent measurement of jet substructure carried out by ALICE using data recorded at the LHC from pp collisions at $\sqrt{s} = 5.02$ or 13 TeV. In particular, Sec. 2 reviews the recent ALICE measurements of the jet angularities, Sec. 3 shows recent ALICE measurements of the jet axis differences, and Sec. 4 discusses the first-ever direct measurement of the dead-cone effect in QCD. Jets were reconstructed using charged-particle tracks and the anti- k_T algorithm³ with E -scheme recombination.

2 Groomed and ungroomed jet angularities

One interesting set of jet substructure observables is the generalized jet angularities λ_α^κ , with

$$\lambda_\alpha^\kappa \equiv \sum_i \left(\frac{p_{T,i}}{p_{T,\text{jet}}} \right)^\kappa \left(\frac{\Delta R_i}{R} \right)^\alpha \equiv \sum_i z_i^\kappa \theta_i^\alpha, \quad (1)$$

where i runs over the jet constituents, R is the jet radius, ΔR_i is the distance from constituent i to the jet axis in the rapidity-azimuth plane, and κ and α are continuous, tunable parameters. These observables are infrared- and collinear- (IRC-)safe when $\kappa = 1$ and $\alpha > 0$, allowing direct calculations from perturbative QCD (pQCD). By varying the angular weighting with α as well as the fragmentation bias with R , one can probe different regions of emission phase space.

ALICE has recently measured⁴ the jet angularities $\lambda_\alpha^{\kappa=1}$ both with and without soft drop grooming for $R \in \{0.2, 0.4\}$ and $\alpha \in \{1, 1.5, 2, 3\}$. Agreement within about 40% is observed with respect to PYTHIA8 Monash 2013⁵ and Herwig 7 (default tune)⁶ Monte Carlo (MC) generators, with noted improvement in the groomed with respect to the ungroomed case. This reflects upon the MC parton shower and fragmentation models, which improve when nonperturbative effects, under less stringent control in the phenomenological approach, are reduced in the grooming step.

Comparisons were also carried out between ALICE data and predictions from Soft-Collinear Effective Theory (SCET)^{7,8}. Nonperturbative corrections were handled in two separate and independent ways. One method was convolution with a nonperturbative shape function⁹ $F(k)$,

$$F(k) = \frac{4k}{\Omega_\alpha^2} \exp\left(-\frac{2k}{\Omega_\alpha}\right) \quad \text{with} \quad \frac{d\sigma}{dp_T d\lambda_\alpha} = \int dk F(k) \frac{d\sigma^{\text{pert}}}{dp_T d\lambda_\alpha} \left(\lambda_\alpha - \frac{k}{p_T R} \right), \quad (2)$$

where k is an integration parameter with units of momentum, p_T is the jet transverse momentum, $\Omega_\alpha = \Omega/(\alpha - 1)$, and Ω is an unknown but presumably universal parameter with units of momentum. This smearing is also followed by a folding to correct for charged-particle jet effects. Figure 1 shows comparisons to theoretical predictions with four different values Ω . Smaller values on the order of 0.2 – 0.4 GeV/ c give the best agreement to the measured spectra. As α is increased and the wider-angle constituents are correspondingly more strongly emphasized, the curves are pushed into the nonperturbative region, and divergence is observed at low λ_α , while the perturbative region remains relatively well-described.

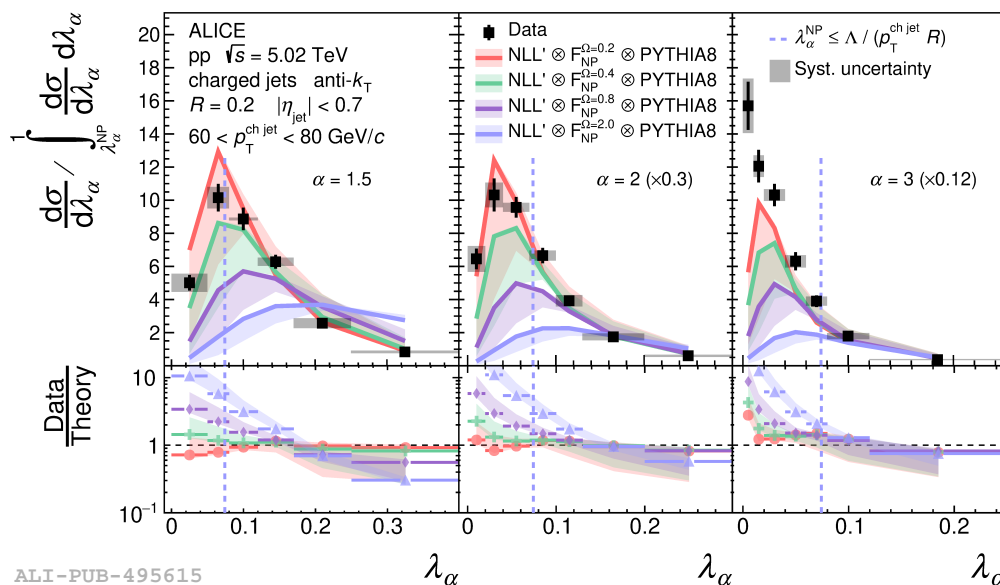


Figure 1 – Example comparison of the ungroomed jet angularities with different values of $\alpha \in \{1.5, 2, 3\}$ to NLL' SCET calculations convolved with different amounts of smearing with a nonperturbative shape function⁴. Distributions are normalized to the perturbative region, right of the vertical dashed line, which uses $\Lambda = 1$ GeV.

3 Jet axis differences

The axis of a jet can be defined in different ways. A standard technique is to use E -scheme recombination, where the 4-vectors of each constituent are summed to obtain the jet 4-vector. One could also follow this approach only using the constituents that survive soft drop grooming. Yet another way is the Winner-Take-All (WTA) method, where the jet is first reclustered into a tree data structure using the Cambridge-Aachen algorithm and then traversed through following the hardest splitting, with the final constituent defining the jet's axis. Measuring the difference between these different jet axis definitions is an IRC-safe way to observe the influence of soft, nonperturbative radiation, and the observable is also sensitive to PDFs and TMDs¹¹.

Measurements of the jet axis differences, ΔR_{axis} , have been carried out by ALICE using the three different definitions above with varying grooming settings. The distributions reveal that the jet axis differences between the standard and groomed axes are strongly correlated, with the distributions spanning a range much smaller than R . The WTA axis, however, tends to be less strongly aligned with the standard or groomed axes, suggesting that p_T tends to be more broadly distributed in the jet, rather than collimated along a single axis.

PYTHIA8 and Herwig 7 are largely able to reproduce these trends, with agreement observed within about 20% for these observables. MC predictions for the WTA differences more closely match ALICE data than the standard-to-groomed ones. Comparisons to NLL' predictions, using charged-particle jet corrections from either MC, also show excellent agreement within uncertainties; an example is given in Fig. 2.

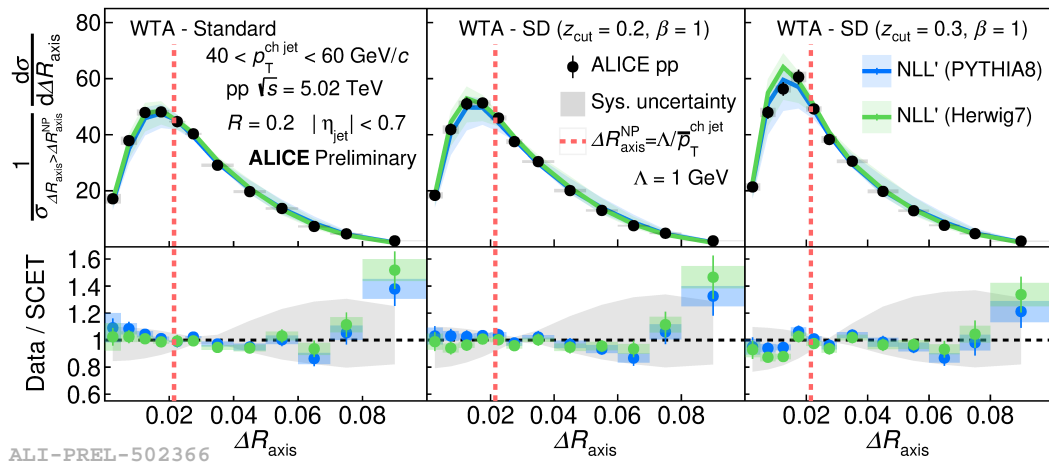


Figure 2 – Example comparison of the WTA with standard and soft drop axes. Theory curves are normalized to the perturbative region, right of the vertical dashed line. Good agreement is observed between data and NLL' calculations in both regions, demonstrating good behavior of the calculations within the given uncertainties.

4 Dead-cone effect in QCD

The dead-cone effect in QCD is the expected suppression of gluon radiation within an angle m/E from an emitting parton¹². Effects can be observed by comparing jets initiated by a heavy-flavor quark with respect to u -, d -, and g -dominated inclusive jets. A direct measurement is challenged, however, by the need to identify gluon radiation separately from secondary effects and to determine the dynamic direction of the quark throughout its parton shower.

ALICE has recently performed the first direct measurement of this effect¹³ by employing the Cambridge-Aachen algorithm to reconstruct the primary Lund plane for both inclusive and D^0 -tagged jets, and then projecting onto the angular axis and taking the ratio between them,

$$R(\theta) = \frac{1}{N^{D^0 \text{ jets}}} \frac{dn^{D^0 \text{ jets}}}{d \ln(1/\theta)} \bigg/ \frac{1}{N^{\text{inclusive jets}}} \frac{dn^{\text{inclusive jets}}}{d \ln(1/\theta)} \bigg|_{k_T, E_{\text{radiator}}} \quad (3)$$

When compared to the light-quark / inclusive limit, significant suppression is seen at small angles, with the suppression also decreasing with E_{radiator} . This effect is also seen in PYTHIA8 and SHERPA MC generators, which is expected. Figure 3 shows the ALICE measurement.

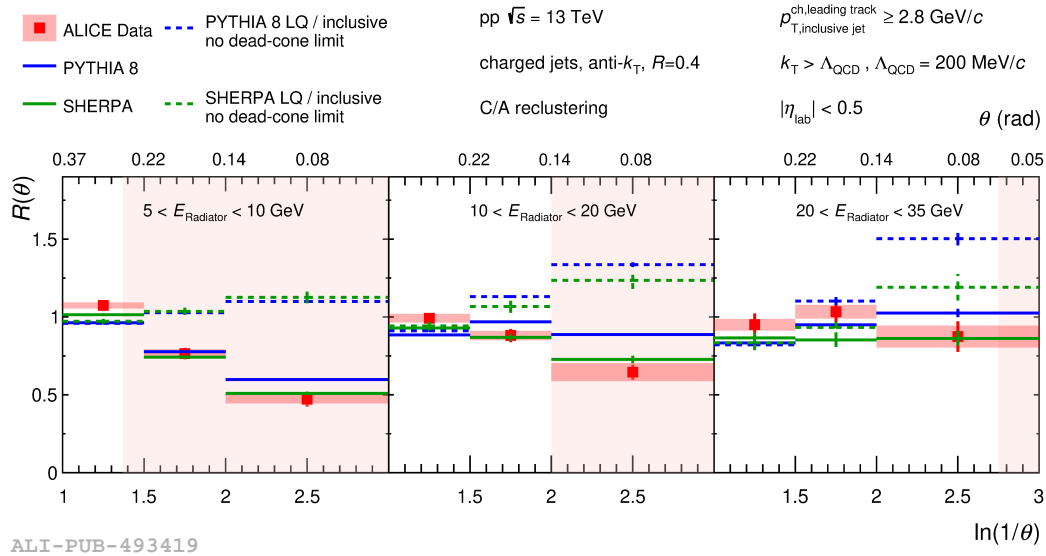


Figure 3 – First direct observation of the dead-cone effect in QCD¹³ using D^0 versus inclusive jets in different bins of E_{radiator} . Small angle suppression corresponds to a dip in the shaded red regions at larger $\ln(1/\theta)$.

References

1. A. J. Larkoski, S. Marzani, G. Soyez, and J. Thaler, “Soft Drop,” *JHEP* **05** 146 (2014), arXiv:1402.2657 [hep-ph].
2. Y. L. Dokshitzer, G. D. Leder, S. Moretti, and B. R. Webber, “Better Jet Clustering Algorithms,” *JHEP* **9708:001** (1997), arXiv:hep-ph/9707323.
3. M. Cacciari, G. P. Salam, and G. Soyez, “The anti- k_t jet clustering algorithm,” *JHEP* **04** (2008) 063, arXiv:0802.1189 [hep-ph].
4. **ALICE** Collaboration, S. Acharya *et al.*, “Measurements of the groomed and ungroomed jet angularities in pp collisions at $\sqrt{s} = 5.02$ TeV,” arXiv:2107.11303 [nucl-ex].
5. T. Sjöstrand *et al.*, “An introduction to PYTHIA 8.2,” *Comput. Phys. Commun.* **191** (2015) 159 - 177, arXiv:1410.3012 [hep-ph].
6. M. Bähr *et al.*, “Herwig++ Physics and Manual,” *Eur. Phys. J. C* **58** (2008) 639–707, arXiv:0803.0883 [hep-ph].
7. Z.-B. Kang, K. Lee, and F. Ringer, “Jet angularity measurements for single inclusive jet production,” *JHEP* **04** (2018) 110, arXiv:1801.00790 [hep-ph].
8. Z.-B. Kang, K. Lee, X. Liu, and F. Ringer, “Soft drop groomed jet angularities at the LHC,” *Phys. Lett. B* **793** (2019) 41 – 47, arXiv:1811.06983 [hep-ph].
9. E.-C. Aschenauer, K. Lee, B. Page, and F. Ringer, “Jet angularities in photoproduction at the Electron-Ion Collider,” *Phys. Rev. D* **101** (2020) 054028.
10. Z.-B. Kang, K. Lee, X. Liu, and F. Ringer, “The groomed and ungroomed jet mass distribution for inclusive jet production at the LHC,” *JHEP* **10** (2018) 137.
11. P. Cal, D. Neill, F. Ringer and W. J. Waalewijn, “Calculating the angle between jet axes,” *JHEP* **04** (2020) 211, arXiv:1911.06840 [hep-ph].
12. Y. L. Dokshitzer, V. A. Khoze, S. I. Troian, “On specific QCD properties of heavy quark fragmentation (‘dead cone’),” *J. Phys. G* **17** (1991) 1602-1604.
13. **ALICE** Collaboration, S. Acharya *et al.*, “Direct observation of the dead-cone effect in QCD,” arXiv:2106.05713 [nucl-ex].